Dark Matter Results from First 98.7-day Data of PandaX-II Experiment

Andi Tan,[2] Mengjiao Xiao,[1] Xiangyi Cui,[1] Xun Chen,[1] Yunhua Chen,[3] Deqing Fang,[4] Changbo Fu,[1] Karl Giboni,[1] Franco Giuliani,[1,5] Haowei Gong,[1] Shouyang Hu,[6] Xingtao Huang,[7] Xiangdong Ji,[1,5,2,*] Yonglin Ju,[8] Siao Lei,[1] Shaoli Li,[1] Xiaomei Li,[6] Xinglong Li,[6] Hao Liang,[6] Qing Lin,[1,†] Huaxuan Liu,[8] Jianglai Liu,[1,‡] Wolfgang Lorenzon,[9] Yugang Ma,[4] Yajun Mao,[10] Kaixuan Ni,[1,§] Xiangxiang Ren,[1] Michael Schubnell,[9] Manbin Shen,[3] Fang Shi,[1] Hongwei Wang,[4] Jiming Wang,[3] Meng Wang,[7] Qiuhong Wang,[4] Siguang Wang,[10] Xuming Wang,[1] Zhou Wang,[8] Shiyong Wu,[3] Xiang Xiao,[1] Pengwei Xie,[1,¶] Binbin Yan,[7] Yong Yang,[1] Jianfeng Yue,[3] Xionghui Zeng,[3] Hongguang Zhang,[1] Hua Zhang,[8] Huanqiao Zhang,[6] Tao Zhang,[1] Li Zhao,[1] Jing Zhou,[6] Ning Zhou,[1,11] and Xiaopeng Zhou[10]

(PandaX-II Collaboration)

[1]*INPAC and Department of Physics and Astronomy, Shanghai Jiao Tong University, Shanghai Laboratory for Particle Physics and Cosmology, Shanghai 200240, China*

[2]*Department of Physics, University of Maryland, College Park, Maryland 20742, USA*

[3]*Yalong River Hydropower Development Company, Ltd., 288 Shuanglin Road, Chengdu 610051, China*

[4]*Shanghai Institute of Applied Physics, Chinese Academy of Sciences, 201800, Shanghai, China*

[5]*Center of High Energy Physics, Peking University, Beijing 100871, China*

[6]*China Institute of Atomic Energy, Beijing 102413, China*

[7]*School of Physics and Key Laboratory of Particle Physics and Particle Irradiation (MOE), Shandong University, Jinan 250100, China*

[8]*School of Mechanical Engineering, Shanghai Jiao Tong University, Shanghai 200240, China*

[9]*Department of Physics, University of Michigan, Ann Arbor, MI, 48109, USA*

[10]*School of Physics, Peking University, Beijing 100871, China*

[11]*Department of Physics, Tsinghua University, Beijing 100084, China*

(Dated: July 27, 2016)

We report the WIMP dark matter search results using the first physics-run data of the PandaX-II 500 kg liquid xenon dual-phase time-projection chamber, operating at the China JinPing Underground Laboratory. No dark matter candidate is identified above background. In combination with the data set during the commissioning run, with a total exposure of 3.3×10^4 kg-day, the most stringent limit to the spin-independent interaction between the ordinary and WIMP dark matter is set for a range of dark matter mass between 5 and 1000 GeV/c^2. The best upper limit on the scattering cross section is found 2.5×10^{-46} cm^2 for the WIMP mass 40 GeV/c^2 at 90% confidence level.

Weakly interacting massive particles, WIMPs in short, are a class of hypothetical particles that came existence shortly after the Big Bang. The WIMPs could naturally explain the astronomical and cosmological evidences of dark matter in the Universe. The weak interactions between WIMPs and ordinary matter could lead to the recoils of atomic nuclei that produce detectable signals in deep-underground direct detection experiments. Over the past decade, the dual-phase xenon time projection chambers (TPC) emerged as a powerful technology for WIMP searches both in scaling up the target mass, as well as in improving background rejection [1–3]. LUX, a dark matter search experiment with a 250 kg liquid xenon target, has recently reported the best limit of 6×10^{-46} cm^2 on the WIMP-nucleon scattering cross section [4], with no positive signals observed. The PandaX-II experiment, a half-ton scale dual-phase xenon experiment at the China JinPing underground Laboratory (CJPL), has recently reported the dark matter search results from its commissioning run (Run 8, 19.1 live days) with a 5845 kg-day exposure. The data was contaminated with significant ^{85}Kr background. After a krypton distillation campaign in early 2016, PandaX-II commenced physics data taking in March 2016. In this paper, we report the combined WIMP search results using the data from the first physics data from March 9 to June 30, 2016 (Run 9, 79.6 live days) and Run 8, with a total of 3.3×10^4 kg-day exposure, the largest reported WIMP data set among dual-phase xenon detectors in the world to date.

The PandaX-II detector has been described in detail in Ref. [5]. The liquid xenon target consists of a cylindrical TPC with dodecagonal cross section (opposite-side distance 646 mm), confined by the polytetrafluoroethylene (PTFE) reflective wall, and a vertical drift distance of 600 mm. For each physical event, the prompt scintillation photons (S1) and the delayed electroluminescence photons (S2) from the ionized electrons are collected by two arrays of 55 Hamamatsu R11410-20 photomultiplier tubes (PMTs) located at the top and bottom, respectively. This allows reconstruction of an event energy and position. A skin liquid xenon region outside of the PTFE

* Spokesperson: xdji@sjtu.edu.cn
† Now at Department of Physics, Columbia University
‡ Corresponding author: jianglai.liu@sjtu.edu.cn
§ Now at Department of Physics, University of California, San Diego
¶ Corresponding author: willandy@sjtu.edu.cn

Setting	live time (day)	E_{drift} (V/cm)	E_{extract} (kV/cm)	PDE (%)	EEE (%)	SEG PE/e	τ_e (μs)
1	7.76	397.3	4.56	11.76	46.04	24.4	348.2
2	6.82	394.3	4.86	11.76	54.43	26.9	393.1
3	1.17	391.9	5.01	11.76	59.78	26.7	409.0
4	63.85	399.3	4.56	11.76	46.04	24.4	679.6

TABLE I: Summary of four settings in Run 9 where E_{drift} and E_{extract} are the drift field in the liquid and electron extraction field in the gaseous xenon, respectively. The fractional uncertainties of the PDE, EEE, and SEG are 5%, 6%, and 3%, respectively, for all settings. Only the average electron lifetime is given in the table, although the S2 vertical uniformity correction was performed for every data taking unit, typically lasting for 24 hours, based on the electron lifetime obtained therein.

wall was instrumented with 48 Hamamatsu R8520-406 1-inch PMTs serving as an active veto. The γ background, which produces electron recoil (ER) events, can be distinguished from the dark matter nuclear recoil (NR) using the S2-to-S1 ratio.

During the data taking period in Run 9, a few different TPC field settings were used to minimize the PMT dark rates and to optimize other running conditions, as summarized in Table I. In each period, calibration runs were taken to study the detector responses. The PMT gains were calibrated using the single photoelectrons (PEs) produced by the low-intensity blue-light pulses transmitted into the detector. To study the multiple PE production in R11410-20 by the approximately 178 nm photons in xenon [6], we measured the PE distributions for individual PMTs using low intensity (<3 PE) physical S1 signals. An average double PE fraction (DPF, defined as the ratio between the occurrence of double PE emission to the total occurrence of non-zero PEs) of 0.21±0.02 was obtained. The response of position-dependent uniformities for S1 and S2 were obtained using the 164 keV γ peaks from meta-stable ^{131m}Xe due to neutron exposure during xenon transportation and the NR calibration. Towards the end of Run 9, the electron lifetime reached 940±50 μs, compared to the 350 μs maximum electron drift time in the TPC. The photon detection efficiency (PDE), the electron extraction efficiency (EEE), and the single electron gain (SEG) and their uncertainties are also shown in Table I.

The analysis reported in this paper follows the procedure as in Ref. [5] with the following major differences. An improved position reconstruction was developed based on a data-driven photon acceptance function (PAF) similar to Ref. [7], leading to a better fiducial volume (FV) definition. We performed NR calibration runs using a low-intensity (approximately 2 Hz) ^{241}Am-Be (AmBe) neutron source with improved statistics, and an ER calibration run by injecting tritiated methane [8], leading to a better understanding of the distributions of the NR and ER events. A boosted-decision-tree (BDT) cut method was developed to suppress accidental background by more than a factor three. Together with a much larger exposure and lower Kr background, these improvements account for the much more sensitive dark matter search result reported here.

Most of external background events locate closer to the wall, therefore a powerful background rejection demands good position reconstruction. In addition to the template matching (TM) algorithm in Ref. [9], a new algorithm was developed based on an iterative fitting of the position-dependent PAF for each PMT. For PMTs located close to the PTFE wall, the PAFs took into account effects due to photon reflections. In each iteration, the position was reconstructed by maximizing the charge likelihood according to the PAF obtained from the previous iteration, and the new position entered into the determination of the next PAF. Using this reconstruction, the Kr events in Run 8 and the tritium calibration events in Run 9 yield good uniformity in the horizontal plane.

The distributions of low energy tritium ER events and AmBe NR events in $\log_{10}$(S2/S1) vs. S1 are shown in Fig. 1. The AmBe calibration was inserted between the dark matter search operation. In total, 3447 of single scatter events were collected. A full Monte Carlo (MC) simulation including neutron-gamma correlated emission from the source, detailed detector geometry, and neutron propagation in and interactions with the detector, and S1-S2 signal production was developed to compare to the data. According to the MC, only <10% of the low energy events are contaminated with multiple scattering in the dead region ("neutron-X"). The data analysis included the neutron-X selections developed in Ref. [9], therefore the final sample was treated as a pure single-scatter NR sample. A fit to the medians of the NR data was performed and compared to the medians obtained from a NEST-1.0 NR model [10] with detector parameters (PDE, EEE, SEG, and DPF) taken into account, resulting in good agreement. The distributions of the NR events in S1 and S2 during AmBe calibration after various selections were compared to the expected distribution based on the MC. Further tuning could improve the agreement for small S1 and S2 between data and simulation (see Fig. 9 in Supplemental Material [[11]]) but worsen the agreement for medians of $\log_{10}$(S2/S1) at low energy, thus untuned NEST will be used when reporting the offical results. The corresponding efficiencies as functions of NR energy are shown in Fig. 2. They were later applied to calculate the dark matter detection efficiency.

Tritiated methane with a specific activity of 0.1 mCi/mmol was administered into the detector through a liquid-nitrogen cold trap, a leak valve, and a 100 ml sample chamber under vacuum, which was flushed with the xenon gas in the detector. We collected a total of 2809 tritium β-decay events. Among these, 9 leaked below the median of the NR band, leading to a leakage fraction of (0.32±0.11)%.

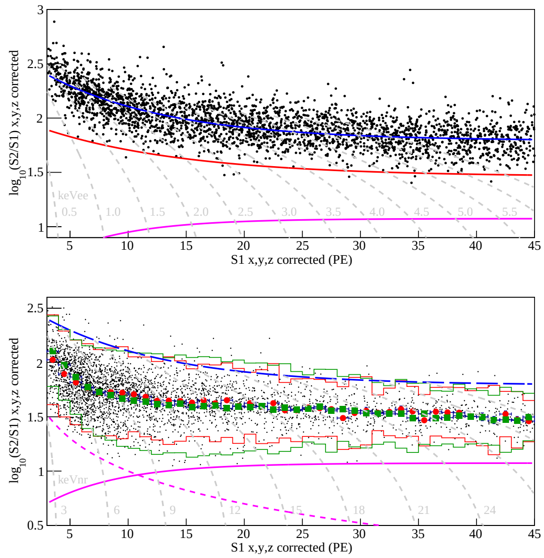

FIG. 1: Top: tritium calibration data in $\log_{10}$(S2/S1) vs. S1, and fits of medians of ER (blue) and NR (red). Bottom: AmBe calibration data in $\log_{10}$(S2/S1) vs. S1, together with medians from the data (red solid circles) and MC (green squares), and the fit to ER medians (blue dashed). The $\pm2\sigma$ boundaries from the data (red lines) and MC (green lines) are overlaid. The dashed magenta curve is the 100 PE selection cut for S2. In both panels, solid magenta curves represent the 99.9% NR acceptance curve from the MC.

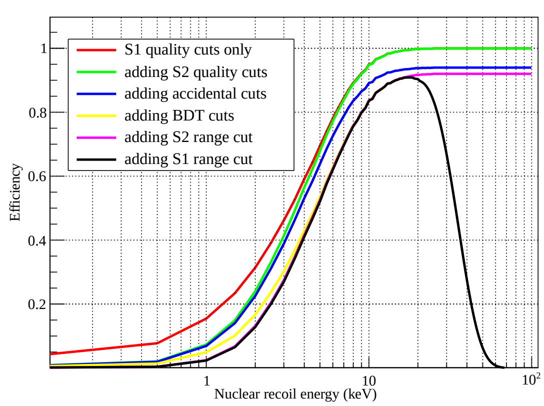

FIG. 2: The detection efficiencies for single-scattering AmBe events as functions of the NR energy after successive applications of selections indicated in the legend.

During the krypton distillation campaign in early 2016, 1.1-ton of xenon was exposed to about one month of sea level cosmic ray radiation, leading to the production of ^{127}Xe, which then decayed via electron capture (EC) to ^{127}I producing characteristic ER energy deposition in the detector. The ^{127}Xe level was identified by the 33 keV L-shell X-ray (following EC). In the low-energy region, M-shell and L-shell vacancies of ^{127}I can produce 1.1 keV and 5.2 keV ER events in the detector, repectively. The background was estimated to be 0.37$\pm$0.05 mDRU (1 mDRU = 10^{-3} events/day/kg/keV$_{ee}$ where keV$_{ee}$ represents "electron equivalent" energy) below 10 keV$_{ee}$ based on the MC by scaling the measured L-shell X-ray rate, in good agreement with 0.31$\pm$0.05 and 0.40$\pm$0.13 mDRU obtained from the spectrum fit and time-dependence fit of the low energy events. The krypton background level was estimated *in-situ* using the β-γ delayed coincidence from ^{85}Kr decay. In total, 52 candidates were identified in Run 9 within 329 kg of fiducial volume (FV, will be discussed later) and no time dependence was observed, leading to an estimate of 44.5$\pm$6.2 ppt of Kr in xenon assuming a ^{85}Kr concentration of 2×10^{-11} in natural Kr. This represents a factor of ten reduction compared to the Kr level in Ref. [5].

The backgrounds due to radio-impurity of detector components shall be the same as those in Ref. [5], and so is the neutron background. The ER background due to Rn was estimated *in-situ* using the β-α and α-α delayed coincidence events. The ^{222}Rn and ^{220}Rn decays were estimated to be 8.6$\pm$4.6 and 0.38$\pm$0.21 μBq/kg, respectively, consistent with the results in Ref. [5]. We also estimated the background from the ^{136}Xe double-β decay events and neutrinos (see Ref. [12] and references therein). The former produces an ER background of 0.10$\pm$0.01 events per 10000 kg-day. The neutrino ER background is dominated by pp solar neutrinos, and is estimated to be between 0.2 and 6.0 events per 10000 kg-day where the lower and upper values assume zero or the current experimental limit of the neutrino magnetic moment [13], respectively. The neutrino NR background was estimated to be 1×10^{-3} events per 10000 kg-day. The final low energy background composition is summarized in Table II.

Item	Run 8 (mDRU)	Run 9 (mDRU)
Total	12.0	1.95
^{85}Kr	11.7	1.19
^{127}Xe	0	0.42
^{222}Rn	0.06	0.13
^{220}Rn	0.02	0.01
Detector material ER	0.20	0.20

TABLE II: Summary of ER backgrounds from different components in Runs 8 and 9. The fractional uncertainties for ^{85}Kr and ^{127}Xe are 17% and 0% for Run 8 and 14% and 25% for Run 9, respectively. The uncertainties for ^{222}Rn and ^{220}Rn in both runs are taken to be 54% and 55%, respectively. The fractional uncertainty due to detector materials is estimated to be 50% based on the systematic uncertainty of the absolute efficiency of the gamma counting station. Different from Ref. [5], values in the table are now folded with detection efficiency.

The accidental background was computed by randomly pairing the isolated S1 (1.8 Hz) and S2 (approximately 1500/day) events. The data quality criteria developed in Ref. [5] removed 67% of random coincidence background. About 15% of the remaining accidental background events are below the NR median. To further suppress this background, selections were developed based on the boosted-decision-tree (BDT) method [14]. The AmBe calibration data and randomly paired isolated S1-S2 signals were used as the input signal and background, respectively. The input data were split into two equal statistics sets, one for training and the other for test. A number of variables for S1 and S2, including the width, shape, charge pattern on the PMTs, and asymmetries between top and bottom array etc., were included in the training. After applying the selections to the test set, the total accidental background was suppressed to 67%, and to 27% for those below the NR median, while the overall AmBe NR efficiency was maintained at 93%. The uncertainty on the accidental background was estimated to be 45% using the difference found in Run 8 and Run 9.

Similar to Ref. [5], the final S1 range cut was chosen to be between 3 to 45 PE, corresponding to an average energy window between 1.3 to 8.7 keV$_{ee}$, and S2s were required to be between 100 PE (raw)and 10000 PE (uniformity corrected). For all events with a single S2, the FV cut was determined based on the PAF-reconstructed position distribution. The selection criterion in the horizontal plane was taken to be $r^2 < 72000$ mm^2. The drift time was required to be between 18 to 310 μs, where the maximum drift time cut was changed from 346 μs in Run 8 to 310 μs to further suppress the below-cathode γ energy deposition (so-called "gamma-X") from ^{127}Xe decays. The liquid xenon mass was estimated to be 329±16 kg, where the uncertainty was estimated based on the position difference between the PAF and TM methods. Note that due to the vertical electric field deformation resulting from the accumulations of wall charges in the TPC [4], the position reconstruction could be distorted near the bottom and out-layers of the TPC, generating non-uniform distributions of the ER calibration events. We have made a conservative choice of the FV here and neglected the field deformation therein. Under these cuts, the final expected background budget is summarized in Table III.

The event rates of Run 9 after successive selections are summarized in Table IV. The skin veto selections are more effective than that in Run 8 since the background was less dominated by the volume-uniform ^{85}Kr β-decays. After the FV cut, 389 events survived. The vertex distribution of all events before and after the FV cut is shown in Fig. 3. The events appear to be uniformly distributed in the FV, showing a small effect of electric field deformation due to wall charges. One event was found below the NR median curve, with its location indicated in Fig. 3. Detailed data quality checks did not reveal artificial issues in this event. The $\log_{10}$(S2/S1) vs.

	ER	Accidental	Neutron	Total Expected	Total observed
Run 8	622.8	5.20	0.25	628±106	734
Below NR median	2.0	0.33	0.09	2.4±0.8	2
Run 9	377.9	14.0	0.91	393±46	389
Below NR median	1.2	0.84	0.35	2.4±0.7	1

TABLE III: The expected background events in Run 8 and Run 9 in the FV, before and after the NR median cut. The fractional uncertainties of expected events in the table are 17% (Run 8 ER), 12% (Run 9 ER), 45% (accidental), and 100% (neutron), respectively. Both the uncertainties from the ER rate and leakage fraction, (0.32±0.11)%, were taken into account in estimating the uncertainty of ER background below the NR median. Number of events from the data are shown in the last column.

S1 distribution for the 389 candidates is shown in Fig. 4. Being close to the NR median line, the single below-NR-median event is consistent with a leaked ER background. Outside the FV, especially in region with large radius, significant events were found with suppressed S2. Similar behaviors were found in the ^{210}Po events (^{222}Rn daughter) originated from the PTFE wall.

Cut	#Events	Rate (Hz)
All triggers	24502402	3.56
Single S2 cut	9783090	1.42
Quality cut	5853125	0.85
Skin veto cut	5160513	0.75
S1 range	197208	2.87×10^{-2}
S2 range	131097	1.91×10^{-2}
Fiducial volume	398	5.79×10^{-5}
BDT cut	389	5.66×10^{-5}

TABLE IV: The event rates in Run 9 after various analysis selections.

The data in Runs 8 and 9 were combined in the final analysis to obtain a new WIMP search limit. The Run 8 data were reanalyzed with the updated reconstruction and data selection cuts except that the vertical cuts were maintained from 20 to 346 μs (FV = 367 kg), since there was no gamma-X contamination from ^{127}Xe in Run 8. This represents the largest dark-matter-search data set among dual-phase xenon detectors to date with an overall exposure of 3.3×10^4 kg-day. A likelihood approach similar to that in Ref. [9] was used to fit the measured data distribution in S1 and S2. A parameterized tritium event distribution were used to simulate expected distributions for different ER background components, and that for accidentals was obtained from the data. The DM NR recoil signals were simulated with the untuned NEST for different WIMP masses as the expected DM distributions, with the conservative low energy cutoff at 1.1 keV$_{nr}$ [4]. The entire data set was separated into

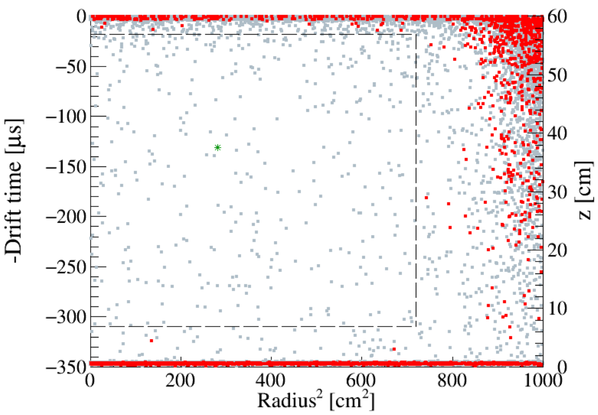

FIG. 3: Position distribution of events that pass all selections (gray points), and those below the NR median (outside FV: red points; inside FV: green star), with FV cuts indicated as the black dashed box.

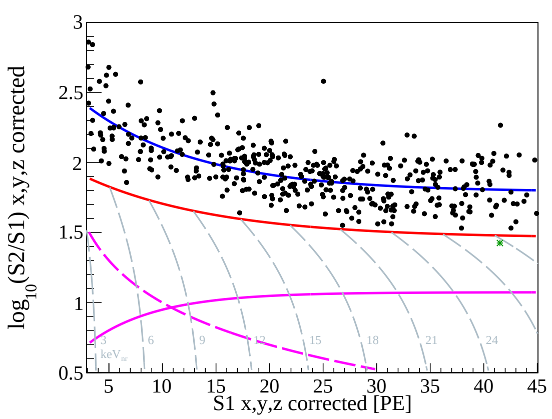

FIG. 4: The distribution of $\log_{10}(S2/S1)$ versus S1 for the dark matter search data. The median of the NR calibration band is indicated as the red curve. The dashed magenta curve represents the equivalent 100 PE cut on S2. The solid magenta curve is the 99.99% NR acceptance curve. The gray dashed curves represent the equal energy curves with NR energy indicated in the figures. The data point below the NR median curve is highlighted as a green star.

15 time bins to take into account time-dependent factors such as the background level and detector parameters (Table I). The overall scales of the four background components, ^{85}Kr, other ER background (including Rn and material background), accidental, and neutron background, were defined as nuisance parameters with nominal values taken from Table II. For ^{127}Xe, on the other hand, the nominal value was derived from the table to include the time dependence for individual time bins. The systematic uncertainties in Tables II and III were used in the corresponding Gaussian penalty terms, which were common to all time bins. To obtain the exclusion limit to spin-independent isoscalar WIMP-nucleon cross section, profile likelihood ratio statistics [15, 16] were constructed over grids of WIMP mass and cross section, and the final 90% confidence level (C.L.) cross section upper limits were calculated using the CL_s approach [17, 18]. The final results are shown in Fig. 5, with recent results from PandaX-II Run 8 [5], XENON100 [19], and LUX [4] overlaid. Our upper limits lie within the $\pm 1\sigma$ sensitivity band. The lowest cross section limit obtained is 2.5×10^{-46} cm^2 at a WIMP mass of 40 GeV/c^2, which represents an improvement of more than a factor of 10 from Ref [5]. In the high WIMP mass region, our results are more than a factor of 2 more stringent than the LUX results [4]. Note that we have been generally conservative in officially reporting the first limits in this article. WIMP NR modeling with a tuned NEST could result in an even more stringent limit (see Fig. 12 in Supplemental Material [[11]]), and a more elaborated treatment of FV cuts would also help.

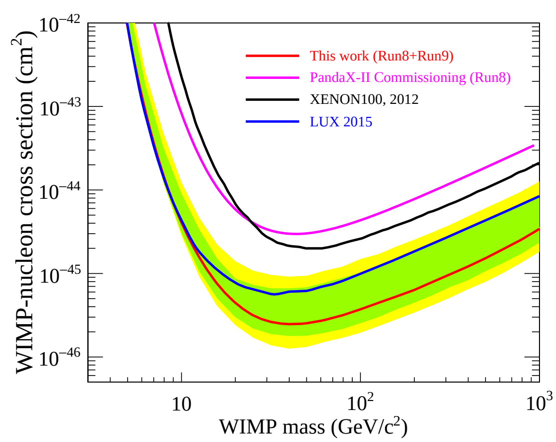

FIG. 5: The 90% C.L. upper limits for the spin-independent isoscalar WIMP-nucleon cross sections from the combination of PandaX-II Runs 8 and 9 (red solid). Selected recent world results are plotted for comparison: PandaX-II Run 8 results [5] (magenta), XENON100 225 day results [19] (black), and LUX 2015 results [4](blue). The 1 and 2-σ sensitivity bands are shown in green and yellow, respectively.

In conclusion, we report the combined WIMP search results using data from Run 8 and Run 9 of the PandaX-II experiment with an exposure of 3.3×10^4 kg-day. No dark matter candidates were identified above background and 90% upper limits were set on the spin-independent elastic WIMP-nucleon cross sections with a lowest excluded value of 2.5×10^{-46} cm^2 at a WIMP mass of 40 GeV/c^2, the world best reported limit so far. The experiment continues to take physics data to explore the previously unattainable WIMP parameter space.

As we were in the final stage of preparing this article, we learnt that the LUX collaboration had released the final result of their experiment at IDM2016 [20], with a similar total exposure and sensitivity.

ACKNOWLEDGMENTS

This project has been supported by a 985-III grant from Shanghai Jiao Tong University, grants from National Science Foundation of China (Nos. 11435008, 11455001, 11505112 and 11525522), and a grant from the Office of Science and Technology in Shanghai Municipal Government (No. 11DZ2260700). This work is supported in part by the Chinese Academy of Sciences Center for Excellence in Particle Physics (CCEPP). The project is also sponsored by Shandong University, Peking University, and the University of Maryland. We also would like to thank Dr. Xunhua Yuan and Chunfa Yao of China Iron & Steel Research Institute Group, and we are particularly indebted to Director De Yin from Taiyuan Iron & Steel (Group) Co. LTD for crucial help on nuclear-grade steel plates. We also thank C. Hall for helping with specifics of tritium calibration. Finally, we thank the following organizations and personnel for indispensable logistics and other supports: the CJPL administration including directors Jianping Cheng and Kejun Kang and manager Jianmin Li, and the Yalong River Hydropower Development Company Ltd.

[1] E. Aprile, C. E. Dahl, L. DeViveiros, R. Gaitskell, K. L. Giboni, J. Kwong, P. Majewski, K. Ni, T. Shutt, and M. Yamashita, Phys. Rev. Lett. **97**, 081302 (2006), arXiv:astro-ph/0601552 [astro-ph].

[2] E. Aprile *et al.* (XENON100), Phys. Rev. Lett. **109**, 181301 (2012), arXiv:1207.5988 [astro-ph.CO].

[3] D. Yu. Akimov *et al.*, Phys. Lett. **B709**, 14 (2012), arXiv:1110.4769 [astro-ph.CO].

[4] D. S. Akerib *et al.* (LUX), Phys. Rev. Lett. **116**, 161301 (2016), arXiv:1512.03506 [astro-ph.CO].

[5] A. Tan *et al.* (PandaX), Phys. Rev. **D93**, 122009 (2016), arXiv:1602.06563 [hep-ex].

[6] C. H. Faham, V. M. Gehman, A. Currie, A. Dobi, P. Sorensen, and R. J. Gaitskell, JINST **10**, P09010 (2015), arXiv:1506.08748 [physics.ins-det].

[7] V. Solovov, V. Belov, *et al.*, IEEE Transactions on Nuclear Science **59**, 3286 (2012).

[8] D. S. Akerib *et al.* (LUX), Phys. Rev. **D93**, 072009 (2016), arXiv:1512.03133 [physics.ins-det].

[9] X. Xiao *et al.* (PandaX), Phys. Rev. **D92**, 052004 (2015), arXiv:1505.00771 [hep-ex].

[10] B. Lenardo, K. Kazkaz, M. Szydagis, and M. Tripathi, IEEE Trans. Nucl. Sci. **62**, 3387 (2015), arXiv:1412.4417 [astro-ph.IM].

[11] Supplmental Material for PandaX-II first data results, `http://pandax.physics.sjtu.edu.cn/articles/supplemental.pdf`.

[12] J. Billard, L. Strigari, and E. Figueroa-Feliciano, Phys. Rev. **D89**, 023524 (2014), arXiv:1307.5458 [hep-ph].

[13] A. G. Beda, V. B. Brudanin, V. G. Egorov, D. V. Medvedev, V. S. Pogosov, E. A. Shevchik, M. V. Shirchenko, A. S. Starostin, and I. V. Zhitnikov, Phys. Part. Nucl. Lett. **10**, 139 (2013).

[14] B. P. Roe, H.-J. Yang, J. Zhu, Y. Liu, I. Stancu, and G. McGregor, Nucl. Instrum. Meth. **A543**, 577 (2005), arXiv:physics/0408124 [physics].

[15] G. Cowan, K. Cranmer, E. Gross, and O. Vitells, Eur. Phys. J. **C71**, 1554 (2011), [Erratum: Eur. Phys. J.C73,2501(2013)], arXiv:1007.1727 [physics.data-an].

[16] E. Aprile *et al.* (XENON100), Phys. Rev. **D84**, 052003 (2011), arXiv:1103.0303 [hep-ex].

[17] A. L. Read, J. Phys. **G28**, 2693 (2002).

[18] T. Junk, Nucl. Instrum. Meth. **A434**, 435 (1999), arXiv:9902006 [hep-ex].

[19] E. Aprile *et al.* (XENON100), Phys. Rev. Lett. **111**, 021301 (2013), arXiv:1301.6620 [astro-ph.CO].

[20] A. Manalaysay *et al.*, in *Identification of Dark Matter 2016* (Sheffield, UK, 2016) `https://idm2016.shef.ac.uk/indico/event/0/contribution/50/material/slides/0.pdf`.